Inductance Impact on Digital Encoding Performance of 850-nm Multimode VCSELs for 50-Gbps NRZ-OOK Data Link

Jui-Hung Weng(1)(2), Wei-Chi Lo(1)(2), Chih-Hsien Cheng(1)(2)(3), Jiaxing Wang(4), Pengfei Qiao(4), Jipeng Qi(4), Chih-Chiang Shen(5), Constance J. Chang-Hasnain(4)(5), Gong-Ru Lin(1)(2)

(1) Graduate Institute of Photonics and Optoelectronics, and Department of Electrical Engineering, National Taiwan University, Taipei, Taiwan R.O.C, grlin@ntu.edu.tw

(2) NTU-Tektronix Joint Research Center, National Taiwan University, Taipei, Taiwan R.O.C

(3) Research Center for Advanced Science and Technology, University of Tokyo, Tokyo 153-0041, Japan.

(4) Pinnacle Photonics Inc. Berkeley, CA 94704 USA

(5) Berxel Photonics Inc. Shenzhen, Guangdong PRC

Abstract *The 50-Gbit/s NRZ-OOK encoding of 850-nm multi-mode VCSEL is achieved by optimizing the contact inductance with shortening transmission-line length from 80 to 25 μm for bandwidth enhancement.*

Introduction

With such rapid development on demanding high-speed vertical-cavity surface emitting laser (VCSEL) for data centers, a versatile fabricating technique such as highly doped and highly reflective distributed Bragg grating mirror, and multi-layer thin-oxide insulated emission aperture, etc. have been successively emerged to provide unique features like large output with low power consumption and high conversion efficiency for multimode VCSELs. However, the finite modulation bandwidth as well as encoding data rate of the multimode VCSEL still limits its practical application. Previously, several approaches were proposed to improve the high-speed characteristics of the multi-mode VCSELs, including the gradually doped grading and DBR scheme for achieving a higher injection density before occurring the thermal rollover effect[1]. Nevertheless, tuning the length of metal padding with adjusting its parasitic inductance to find out the optimal design of VCSEL has yet to be studied for high-speed modulation. The simplified circuit model is used to analyze the extrinsic response limited by chip parasitics[2].

In contrast to the aforementioned works, the simplified circuit model including the capacitance and the padding inductance which affect extrinsic response will be discussed to compare the change caused by varying the length of microstrip transmission line. The microwave transmission-line structured contact design with inductance optimization is demonstrated in this work for improving the analog modulation bandwidth and the NRZ-OOK data rate of the multimode VCSEL. Particularly, the size of the confined oxide aperture and the length of the transmission-line inductor for improving the data transmission performance. By analyzing the reflection coefficient and -3dB bandwidth of analog modulation affected via different designs, the optimized device with the most flattened modulation throughput and the least relative intensity noise (RIN) is selected for PAM-4 data transmission. With employing waveform pre-emphasis, 50-Gbit/s NRZ-OOK and 84-Gbit/s PAM-4 are successfully delivered by such a specific 850-nm MM-VCSEL.

Experimental setup

The cross-sectional structure of the newly designed MM-VCSEL is shown in Fig. 1(a), in which the heterostructure in active region with 5 pairs of $In_{0.072}Ga_{0.928}As$ multi-quantum-wells (MQWs) separated by 6 layers of $Al_{0.37}Ga_{0.63}As$ barrier. Afterwards, 2 pairs of $Al_{0.98}Ga_{0.02}As/Al_{0.12}Ga_{0.88}As$ and 4 pairs of $Al_{0.96}Ga_{0.04}As/Al_{0.12}Ga_{0.88}As$ respectively grow on the bottom and top of the mesa to enhance the optical confinement. The emission window within the mesa is configured with a diameter of 7.5-μm after shrinking by introducing bi-layer-oxide isolation. Moreover, 14 pairs of $Al_{0.9}Ga_{0.1}As/Al_{0.12}Ga_{0.88}As$ p-type DBR and 8 pairs of $Al_{0.9}Ga_{0.1}As/Al_{0.12}Ga_{0.88}As$ n-type DBR with 25 pairs of undoped $AlAs/Al_{0.1}Ga_{0.9}As$ were respectively constructed as top and bottom mirrors to form the cavity of the MM-VCSEL.

Fig. 1(b) shows the image that the p-type top surface of MM-VCSEL was metallic contacting by an Au hemi-ring connected to the circular pad with using microstrip transmission lines of different lengths, where the devices A and B are denoted with a transmission line length of 80 and 25 μm, respectively. To compare the effect of the confined oxide aperture size on the high-speed data encoding performance, different aperture diameters of 7 and 7.5 μm are designed for A and

978-1-6654-3868-1/21/$31.00 ©2021 IEEE

B devices.

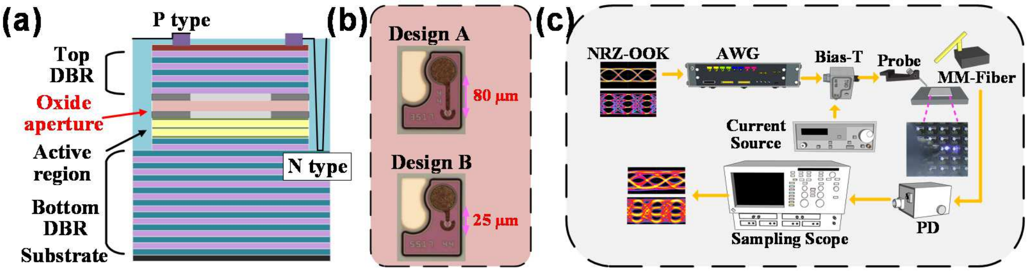

Fig. 1: (a) The cross-sectional structure of MM-VCSEL, (b) the top-view of MM-VCSEL, (c) the setup for NRZ-

Fig. 1(c) demonstrates the experimental setup for testing the NRZ-OOK and PAM-4 data transmissions carried by the 850-nm MM-VCSEL. Both NRZ-OOK and PAM-4 data formats were generated by an arbitrary waveform generator (AWG, Keysight M8194A) at a sampling rate of 120 GS/s. The DC bias supplied by the current source (ILX Lightwave LDX-3210) for tuning the bias condition of the MM-VCSEL was coupled with the data stream via a 65-GHz bias-tee (Anritsu, V250). The MM-VCSEL was precisely controlled at 20°C using the liquid-cooling heat sink. A 40-GHz broadband ground-signal probe (GGB, 40A-GS-125-DP) was used to turn on and directly modulate the MM-VCSEL. The VCSEL output was picked up by a lensed MMF with 50-μm core and converted back to an electrical signal via a 22-GHz photodetector (New Focus, 1484-A-50). A digital serial analyzer (DSA, Tektronix 8300) was used to analyze the eye diagrams in NRZ-OOK and PAM-4 formats. The decoding bit-error-rate (BER) was calculated by the demodulated program (80SJNB) embedded in the DSA.

Results and Discussions

Fig. 2(a) and 2(b) reveals the P-I-V, dP/dI, and dV/dI of the MM-VCSELs with sample numbers of A-OA-7 and B-OA-7. With extracting the threshold current and linear modulation range from first-order differential plots, the rollover effect is observed to induce the significant output saturation at I_{bias} > 15 mA (~25 I_{th}) for sample A-OA-7 and I_{bias} > 14 mA (~23 I_{th}) for sample B-OA-7, as shown in the left parts of Fig. 2(a) and 2(b). The differential resistance of the VCSEL operated beyond the threshold of the MM-VCSEL remains as large as 127 Ω for A sample and 120 Ω for B sample, which gradually reduces to 68.7 Ω for A-OA-7 and 66 Ω for B-OA-7 when biasing the MM-VCSEL as high as 13 mA (~21 I_{th}). Fig. 2(c) depicts the analog modulation response of the MM-VCSELs. In experiment, the small-signal modulation reveals that all the A devices exhibit higher throughput but smaller bandwidth than B. At optimized DC biased conditions, the B devices with the shorter transmission-line contact provides the lower inductance at higher frequency to enhance their -3dB analog bandwidth. By the oxide-confined aperture size as 7 μm, the VCSEL enlarges its modulation bandwidth from 19.2 to 21.3 GHz by shortening its transmission-line length from 80 to 25 μm for B device. With increasing the isolated oxidation area to shrink the aperture from 7.5 to 7 μm, the carrier density enlarges in the smaller emission area (7 μm) to effectively broaden the bandwidth, whereas the larger emission aperture (7.5 μm) not only causes the higher lasing threshold but also suffers from the larger thermal effect in emission core to cause the smaller -3dB bandwidth.

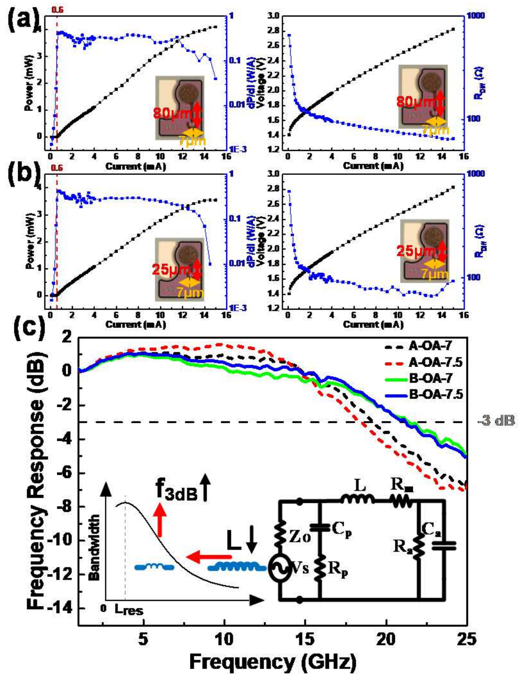

Fig. 2: (a) P-I-V curves of A-OA-7, (b) P-I-V curves of B-OA-7, (c) the frequency responses in all designs.

In general, the correlation between the padding inductance and the modulation bandwidth of the VCSELs exhibits a resonance at specific frequency, as shown in Fig. 2(c), where the interaction of inductance and capacitance provides the widest bandwidth. Such a change is dominated by the serial connected L and the parallel connected R_a and C_a. Tuning the inductance of metal padding would benefit the best fitting with the capacitance effect in active region to broaden the modulation bandwidth of the VCSEL with design B. As an evidence, the measured -3dB bandwidth of the VCSEL in design A correlates well with the simulation derived from transfer function, which will decrease by increasing L in the equivalent circuit of VCSEL. The Table.1 lists the differential resistance, conversion efficiency and -3dB bandwidth of different VCSELs at their optimized biases.

Tab. 1: The characteristics of MM-VCSEL in four designs.

Device	dV/dI(Ω)	dP/dI(W/A)	f_{3dB} (GHz)
A-OA-7	80.3	0.22	19.2
A-OA-7.5	71.6	0.47	18.3
B-OA-7	76.4	0.25	21.3
B-OA-7.5	67.5	0.36	21.1

To find out the optimized DC bias, the signal-to-noise ratio (SNR) of the encoded NRZ-OOK data versus bias current and data amplitude are analysed in Fig. 3(a).

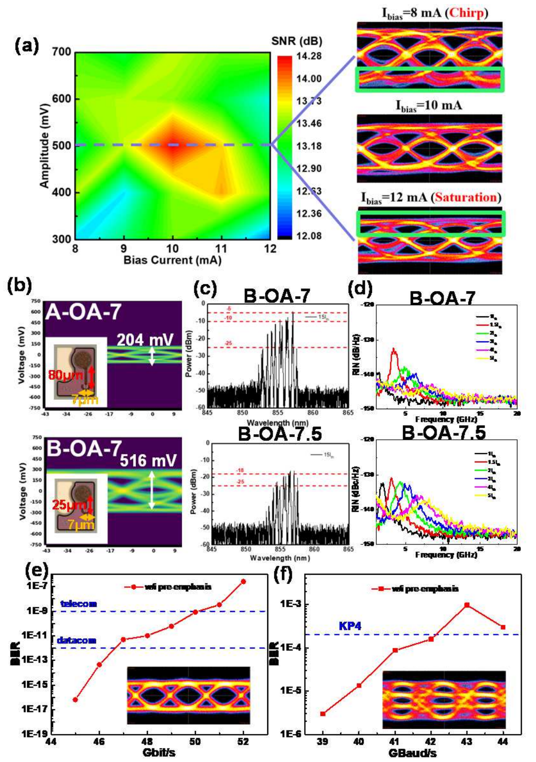

Fig. 3: (a) The SNR contour map and selected eye-diagram at different bias in B-OA-7. (b) The eye-diagram with same input amplitude in A-OA-7 / B-OA-7. (c) the optical spectrum, (d) the RIN spectrum in B-OA-7 / B-OA-7.5. The BER vs modulation bandwidth for (e) NRZ-OOK and (f) PAM-4 in B-OA-7.

At a constant peak-to-peak amplitude of 500 mV, the distortion in the bottom of the received eye diagram is attributed to the dynamic frequency chirp as induced by direct modulation under low DC bias, whereas the waveform clipping induced distortion at the top of the eye diagram occurs due to the saturation of the P-I curve. With such a SNR contour-mapping analysis, the operation point of the B-OA-7 VCSEL is optimized at 10 mA and 500 mV for obtaining the highest SNR. The different oxide aperture design results in a discrepancy between their resistance since the extra oxidation region also increase additional resistance across the isolation region of devices. In addition, the microstrip transmission line pad also performs as a serially connected resistance and inductance. Since short padding in design B reveals a lower resistance than design A which is closer to 50 Ω to facilitate impedance matching with a smaller voltage standing wave ratio (VSWR), the lengthened microstrip transmission line pad with a high reflection coefficient in design A suppresses its modulation depth, whereas the modulation throughput of design B becomes greater than design A under the same input amplitude in Fig. 3(b).

By operating the B devices at constant DC bias and data amplitude, Fig. 3(c) and 3(d) compares their lasing mode spectra, relative intensity noise. Since the lower photon density in the B-OA-7.5 with a larger aperture diameter will contribute to higher RIN, B-OA-7 becomes a candidate for high-speed transmission. Fig. 3(e) and 3(f) describes the relationship between data rate and receiving BER after employing pre-emphasis, showing that 50-Gbit/s NRZ-OOK is successfully transmitted by B-OA-7 with the BER of 8.3×10^{-10} to meet the telecom required BER criterion 10^{-9}. For PAM-4 data format, the B-OA-7 also enables 42-Gbaud/s transmission with the BER of 1.6×10^{-4} which satisfies the KP4-FEC criterion.

Conclusion

The 50 Gbit/s NRZ-OOK is successfully achieved by the 850-nm MM-VCSEL. According to -3dB BW and modulation depth which are controlled by different designs in oxide aperture size and length of padding, we choose the candidate for high-speed transmission in our four designs. At the optimized bias current at 10 mA (~$17I_{th}$), the MM-VCSEL has a conversion efficiency of 0.25 W/A, differential resistance of 76.4 Ω, 3dB BW of 21.3 GHz, RIN peak power of －134.42 dBc/Hz. After performing the pre-emphasis technique, 50 Gbit/s NRZ-OOK can be satisfied with telecom required BER criterion, and 42 Gbaud/s PAM-4 support 84 Gbit/s data throughput can meet the KP4-FEC.

References

[1] P. Westbergh *et al.*, "High-Speed Oxide Confined 850-nm VCSELs Operating Error-Free at 40 Gb/s up to 85°C", *IEEE Photonics Technol. Lett.*, vol. 25, pp. 768–771, Apr. 2013.

[2] W. Hamad *et al.*, "Impedance Characteristics and Chip-Parasitics Extraction of High-Performance VCSELs", *IEEE J. Quantum. Electron.*, vol. 56, no. 1, Feb. 2020.